Active Control of Flow Noise Sources in Turbulent Boundary Layer on a Flat-Plate Using Piezoelectric Bimorph Film

Woo-Seog Song, Seungbae Lee*
Department of Mechanical Engineering, College of Engineering, Inha University, Incheon 402-751, Korea
Dong-Shin Shin
Department of Mechanical System Design Engineering, College of Engineering, Hongik University, Seoul 121-791, Korea
Yang Na
CAESIT, Department of Mechanical Engineering, Konkuk University, Seoul 143-701, Korea

The piezoelectric bimorph film, which, as an actuator, can generate more effective displacement than the usual PVDF film, is used to control the turbulent boundary-layer flow. The change of wall pressures inside the turbulent boundary layer is observed by using the multi-channel microphone array flush-mounted on the surface when actuation at the non-dimensional frequency $f_b^+=0.008$ and 0.028 is applied to the turbulent boundary layer. The wall pressure characteristics by the actuation to produce local displacement are more dominantly influenced by the size of the actuator module than the actuation frequency. The movement of large-scale turbulent structures to the upper layer is found to be the main mechanism of the reduction in the wall- pressure energy spectrum when the $700\nu/u_\tau$-long bimorph film is periodically actuated at the non- dimensional frequency $f_b^+=0.008$ and 0.028. The biomorph actuator is triggered with the time delay for the active forcing at a single frequency when a 1/8″ pressure-type, pin-holed microphone sensor detects the large-amplitude pressure event by the turbulent spot. The wall-pressure energy in the late-transitional boundary layer is partially reduced near the convection wavenumber by the open-loop control based on the large amplitude event.

Key Words : Flow Control, Piezoelectric Bimorph, Wavenumber-Frequency Spectrum

Nomenclature

Δx^+ : Normalized streamwise length ($\equiv u_\tau \Delta x/\nu$)
Δz^+ : Normalized spanwise length ($\equiv u_\tau \Delta z/\nu$)
f_b^+ : Mean bursting frequency ($\equiv f\nu/u_\tau^2$)
U_0 : Flow velocity
U_c : Convective velocity
u_τ : Friction velocity
ν : Viscosity
d^+ : Non-dimensional pin-hole diameter ($\equiv u_\tau d/\nu$)
Re_θ : Reynolds number based on momentum thickness
k_x : Streamwise wavenumber (rad/m)
τ_ω : Mean wall shear-stress

* Corresponding Author,
E-mail : sbaelee@inha.ac.kr
TEL : +82-32-860-7325; **FAX** : +82-32-868-1716
School of Mechanical Engineering, Inha University, 253, Yonghyun-dong, Nam-gu, Incheon 402-751, Korea. (Manuscript **Received** May 1, 2006; **Revised** August 4, 2006)

1. Introduction

Recently, the rapid increase of energy cost and environmental concerns have revitalized the research of drag reduction and flow noise control in areas of transportation vehicle and turbomachinery etc. The effective schemes for turbulent

active control have been presented in relation to numerical methods of LES (Large-Eddy Simulation) and DNS (Direct Numerical Simulation), which were summarized in the review papers by Gad-el-Hak (2000) and Collis (2004).

Many turbulent motions are known to have coherent structures. The coherent structures in the turbulent boundary layer near the wall contribute to 80% of overall fluctuating energy and transfer their energy to the smaller scales through ejection, bursting, and sweep motions, and thereby, increase the Reynolds stresses, which act as a major factor of drag increase.

The turbulent boundary layer generates two types of pressure fluctuations : near-field pressure fluctuations confined in the boundary layer and pressure fluctuations of low-wavenumbers radiating to the far-field. With respect to the sound source, the dipole source is cancelled by the image effect of the wall, and the longitudinal quadrupole source from Reynolds stresses is enhanced by the presence of the wall (Powell, 1960). Wang et al.(1996) argued that the quadrupole source is closely related to the vortex structure breakdown occurring in the high shear-layer and to the production of Reynolds stress by hair-pin eddy shedding in the transitional boundary layer. Lee et al.(1999) discussed the large amplitude events of wall pressure fluctuations in the turbulent boundary layer, which radiate to the far-fields in case of satisfying the radiation condition.

A control scheme that reduces the activity of the coherent structure is considered to have the ability to reduce the radiated sound from large-amplitude events on the wall. Thus, the effective actuator for disturbing the flow structures and the control algorithm based on spatial-temporal information measured from sensors have been studied extensively. The specification needed for flow-control actuators may be summarized by fast time response, reliability, low power consumption, and low cost. Therefore, the piezoelectric actuator has been assumed to be the best candidate since Wehrmann (1965, 1967). Wiltse and Glezer (1993) devised an excitation scheme for piezoelectric actuators by using an amplitude modulation (AM) method. Jacobson and Reynolds (1998) reported the reduction of wall shear-stress in the laminar boundary layer by 8% with an actuator consisting of a cavity and a piezoelectric ceramic.

Smith and Glezer (1998) studied the effect of vortex introduced by a synthetic jet on the turbulent boundary layer by using a piezoelectric device with a cavity. Jeon and Blackwelder (2000) measured the disturbed flow by a delta-shaped piezo-ceramic actuator in the turbulent boundary layer. But all the piezo-ceramic actuators used in the previous studies could produce large-amplitude actuations only near their resonance frequencies which are determined by material properties, not the sort of disturbances in a broad range of frequency.

In this study, a piezoelectric bimorph actuator for wall deformation was designed to generate disturbances in a broad range of frequency, and was applied to control late transitional flow and fully developed flow on a flat surface. The wall pressures inside the turbulent boundary layer downstream of the actuator were measured by using a multi-channel microphone array flush-mounted on the surface, and their wavenumber-frequency spectra were analyzed and discussed.

2. Experimental Set-up and Measurements

The experiment was conducted in an anechoic wind tunnel with an open test section that measures 400 mm wide and 400 mm high, and the maximum speed at the test section was 30 m/s. The maximum value of turbulence intensity on the order of 0.25% and total pressure variations on the order of 0.2% were measured and were considered adequate to prevent any spurious effects on aerodynamic coefficients. A more detailed description of the wind tunnel is provided in Lee et al.(1999).

To measure the velocity profile in the boundary layer on the surface, an I-type hot-wire probe (DANTEC55P15) was automatically traversed within the accuracy of 1/50 mm in two perpendicular directions. The calibration between the voltage and the velocity was based on a fourth-

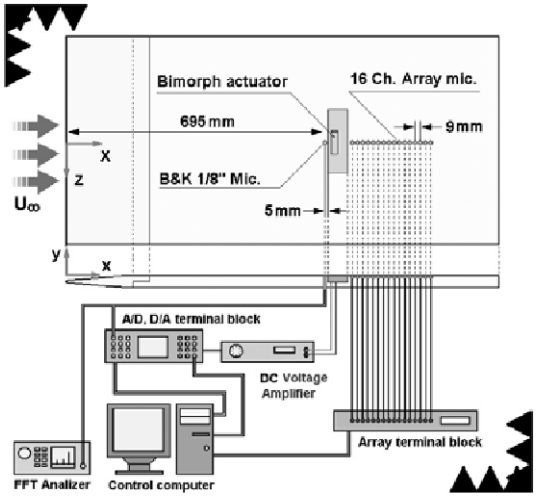

Fig. 1 Control system setup

order polynomial, and 300,000 data were acquired for 30 seconds to obtain a mean velocity at a specified position. The wall-friction coefficient was computed by using the CPM (Computational Preston-tube Method).

Figure 1 shows the bimorph film on the wall and the array of microphones flush mounted on the surface downstream of the film. The hard wall used in the experiment had a width of 700 mm and length of 1,280 mm and was made of an acrylic material. The two actuators of the piezoelectric bimorph had the dimensions of 1400 v/u_τ, 700v/u_τ, respectively, in the streamwise direction with the same thickness of 52 μm, and were located 700 mm downstream from the leading edge. The spatial period for the low-speed vortex streaks near the wall was estimated as 20 mm for the condition of experiment by considering the average distance Δx^+ of the structures to be 1,000. To identify the effect of the module size on the structures, the effective length of the film was set to 0.7 (shorter) and 1.4 (longer) times the average streamwise length.

The forcing frequencies, which were computed, satisfied the conditions of $f_b^+=0.008$, 0.028 based on the measured wall-friction coefficient, and the electric signals at those frequencies were applied to the piezoelectric bimorph films. The frequencies $f_b^+=0.008$ and $f_b^+=0.028$ correspond to twice the bursting frequency (Blackwelder et al., 1983) close to the measured frequency of large-amplitude events and the upper limit frequency for effective actuation, respectively. The DC voltage for forcing the piezoelectric bimorph film was supplied by HA400A (Eliezer Co.).

The 1/8″ pressure-type microphone sensor (B&K 4138), which had a non-dimensional pin-hole diameter d^+ of approximately 7.1 and was located 695 mm downstream from the leading edge of the plate, was used to measure the events in the boundary layer. An array of 16 microphones, which had diameter of 8 mm and height of 25.4 mm, were all connected to a 16-channel signal amplifier. Each microphone was 9 mm apart and the whole set spanned 135 mm. To increase the spatial resolution, the pressure-releasing hole of 0.8mm on the cover of the microphone array was set over the center of each microphone. The data from each channel were recorded for 20 seconds with the data length of 20,000 per one second. The pressures were processed through the temporal-spatial Fourier transform suggested by Keith et al.(1991), and 240 Fourier- transforms were used for averaging.

In the first step, the module size and the actuation frequency were determined by analyzing the temporal-spatial Fourier transform for each case. In the second step, the data obtained were processed with an AD/DA board of dSPACE Real Time Interface 1104, and the active control was implemented on Control Desk driven by Matlab Simulink software, where the frequency, the amplitude, and the threshold of the output were specified with consideration of the time delay for the convection effect.

3. Experimental Results and Discussion

3.1 Characteristics of bimorph actuator and mode analysis

A bimorph film moves in the transverse direction because of the two PVDF films bonded at both ends, otherwise deforming on the plane. The bonded film is more effective for generating deformation or forcing than a single PVDF film of

Table 1 Specification of PVDF actuator

Piezo film thickness	28 μm
Bimorph thickness	56 μm
Maximum input voltage	500 V DC, 250 V$p-pAC$
Storage temperature	−40℃ ~ 70℃
Operating temperature	0℃ ~ 70℃
Electrode	Elastomeric Ag ink
Displacement	2 μm per volt at tip

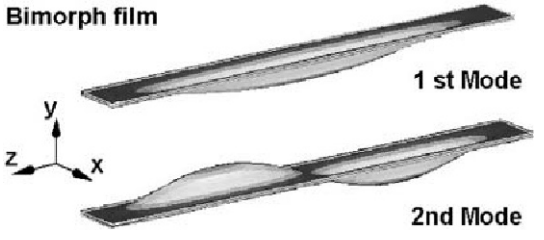

Fig. 2 Mode analysis of bimorph film by Ansys[T.M.] software

separated poles, and its response is fast over a wide range of input. It may be suitable for precise positioning and vibration control due to its ability of precise sensing and actuation. The details of the bimorph film used for actuation in this study are given in Table 1. Because its dynamic characteristics depend on the installation condition, modal analysis was performed to identify the dynamic behavior of the bimorph film by using ANSYS[T.M.] software. The boundary condition was set such that no displacement occurred at the four corners for the voltage difference of 100 V across the film. Two types of standing mode were observed for the material properties and the boundary condition as shown in Fig. 2, and the amplitude of the second mode was negligible compared to the first one, thus confirming the applicability of the film as an actuator.

3.2 Wall-pressure characteristics in the turbulent boundary layer by local wall vibration

Figure 3 and Table 2 shows the fully-developed velocity distribution and its turbulent characteristics at 700 mm downstream of the leading edge by the external speed of 14.44 m/s. The normalized wavenumber spectrum at $\omega\delta^*/U_o=0.453$, which was measured on the rigid surface, was compared with that of Abraham and Keith (1998), as shown in Fig. 4. Note that the peak $k_x\delta^*$ coincides with each other, but the background level of present experiment is higher than of Abraham and Keith.

Table 2 Boundary layer parameters

U_0 (m/s)	14.440
Density (kg/m^3)	1.1653
Viscosity (m^2/s)	1.5925E-05
τ_w (kg/ms^2)	0.5271
Shape Factor	1.3997
u_τ (m/s)	0.7416
Re_θ	1548

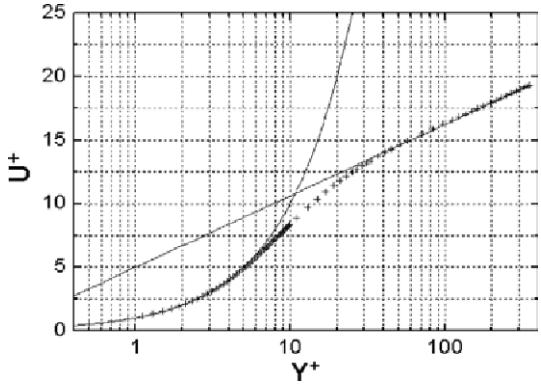

Fig. 3 Velocity profiles on rigid plate at $x=700$ mm ($Re_\theta=1548$)

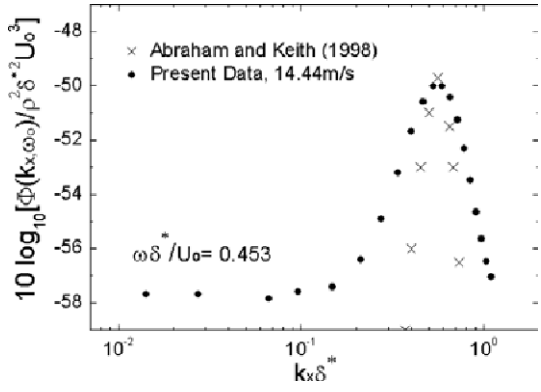

Fig. 4 Comparison of normalized wavenumber-frequency spectra

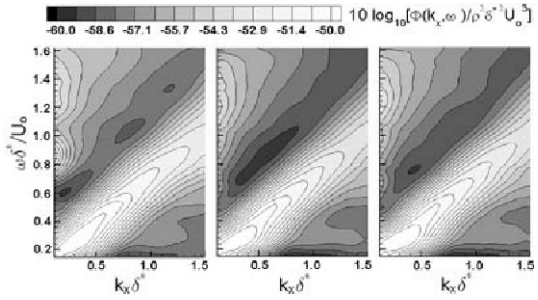

(a) rigid plate (b) $f_b^+=0.008$ (c) $f_b^+=0.028$

Fig. 5 Wavenumber-frequency spectra for rigid wall and deformed walls actuated by $1400\nu/u_\tau$-long module

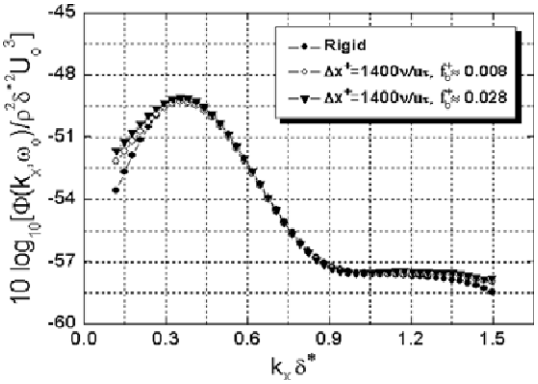

Fig. 6 Wall-pressure energies in terms of normalized wavenumber at $\omega\delta^*/U_o=0.30$ in Fig. 5

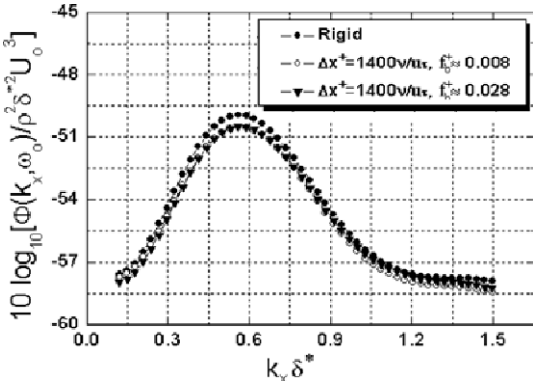

Fig. 7 Wall-pressure energies in terms of normalized wavenumber at $\omega\delta^*/U_o=0.45$ in Fig. 5

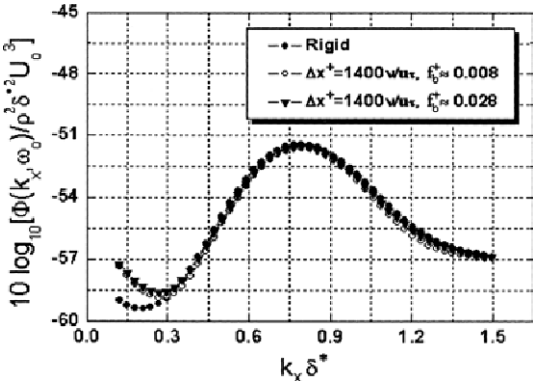

Fig. 8 Wall-pressure energies in terms of normalized wavenumber at $\omega\delta^*/U_o=0.60$ in Fig. 5

The normalized temporal-spatial spectra of the wall pressure, when activated by the $1400\nu/u_\tau$-long module at the frequency $f_b^+=0.008$ and 0.028, were compared with that of the solid surface without forcing in Fig. 5. Figure 5(a) shows the temporal-spatial energy spectra of wall pressure on the solid surface. The high wall-pressure energy pattern of the low-wavenumber, low-frequency component is observed to spread out as a fan shape to the high-wavenumber and the high-frequency components with the manifesting convection ridge of $U_c/U_o\sim0.75$, which is very typical for convecting turbulence structures. The results of cases of $f_b^+=0.008$ and 0.028 did not change significantly from that of the case of the rigid wall, as shown in Fig. 5(b) and Fig. 5(c).

The wall pressure energies in the wavenumber domain are compared at $\omega\delta^*/U_o=0.30, 0.45$, and 0.60 for the forcing and the non-forcing cases in Figs. 6-8, respectively. Only slight reduction of energy is identified at the convective wavenumber $k_c\delta^*=0.56$ for both actuation cases at $\omega\delta^*/U_o=0.45$. From the relation $U_c=\omega/k_c$, the characteristic turbulence structures are assumed to convect at the speeds of $0.83U_o$, $0.80U_o$, and $0.76U_o$ for the cases of $\omega\delta^*/U_o=0.30$, 0.45, 0.60, respectively.

Figure 9 shows the normalized temporal-spatial spectra of wall pressures, when activated by the $700\nu/u_\tau$-long module at the frequency $f_b^+=$ 0.008 and 0.028. They are also compared with that of solid surface case without forcing in the figure. As shown in Fig. 9(b) and Fig. 9(c), the temporal-spatial spectra of wall pressures have some wiggles on the convection ridge in the area of low-wavenumber, low-frequency and show relatively low energies. Figures 10~12 reproduce the

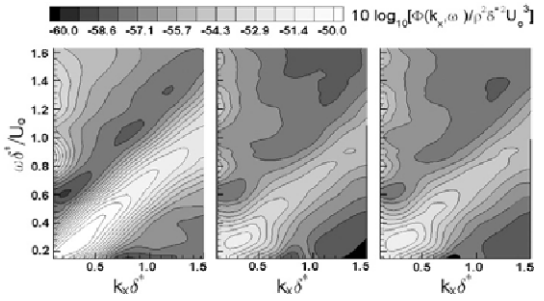

(a) rigid plate (b) $f_b^+=0.008$ (c) $f_b^+=0.028$

Fig. 9 Wavenumber-frequency spectra for bimorph actuator of $700v/u_\tau$-long module

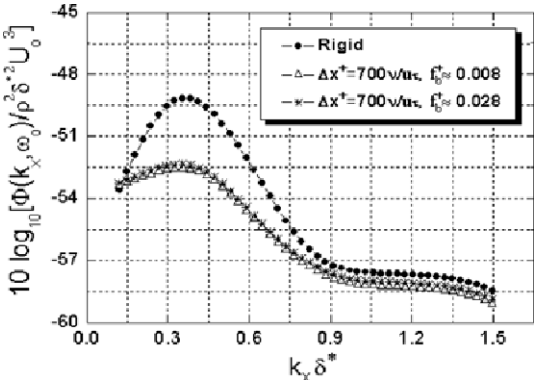

Fig. 10 Wall-pressure energies in terms of normalized wavenumber at $\omega\delta^*/U_o=0.30$ in Fig. 9

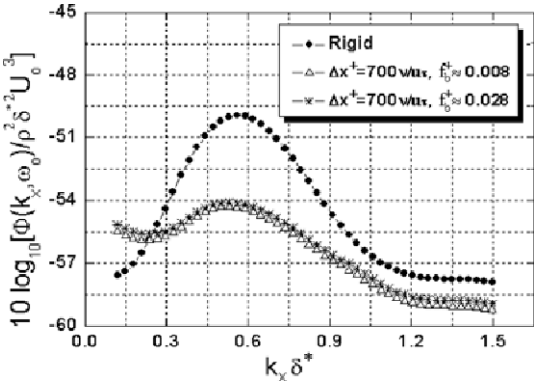

Fig. 11 Wall-pressure energies in terms of normalized wavenumber at $\omega\delta^*/U_o=0.45$ in Fig. 9

normalized wall pressure energies in the wavenumber domain at the normalized frequency $\omega\delta^*/U_o=0.30$, 0.45, 0.60, respectively. The convection speeds corresponding to convection wavenumber

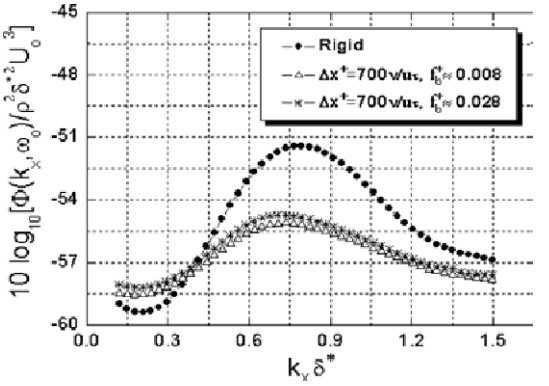

Fig. 12 Wall-pressure energies in terms of normalized wavenumber at $\omega\delta^*/U_o=0.60$ in Fig. 8

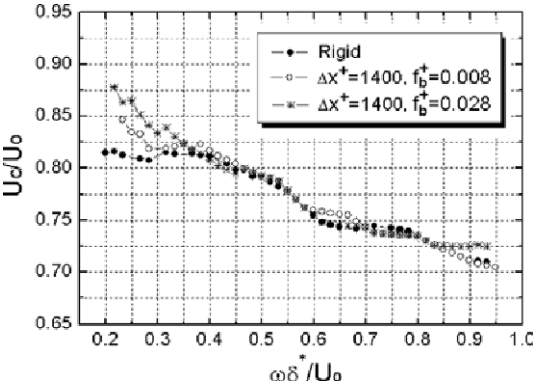

Fig. 13 Convection speed at each normalized frequency of wall-pressure spectrum by $1400v/u_\tau$-long bimorph actuator

$k_c\delta^*=0.35$, 0.53, 0.74 are $0.87U_o$, $0.85U_o$, and $0.82U_o$ for the cases of $\omega\delta^*/U_o=0.30$, 0.45, 0.60, respectively. The forcing cases of $f_b^+=0.008$ and 0.028 resulted in significant energy reductions in the region near the convection wavenumber.

The convection speed at each $\omega\delta^*/U_o$ is summarized in Fig. 13 for the case of $1400v/u_\tau$-long module. The rigid wall is found to have the decreasing pattern of convection speed from 0.82 to 0.70 for $0.2\leq\omega\delta^*/U_o\leq0.95$. The $1400v/u_\tau$-long module is only effective for the change of convection speed of very large-scale structure. Note that the turbulent structures in the viscous sub-layer and the outer-layer contribute to the high- and low-frequency energy spectra, respectively (Choi et al., 1990; Farabee, 1991). Thus, the actuation drives very large structures of

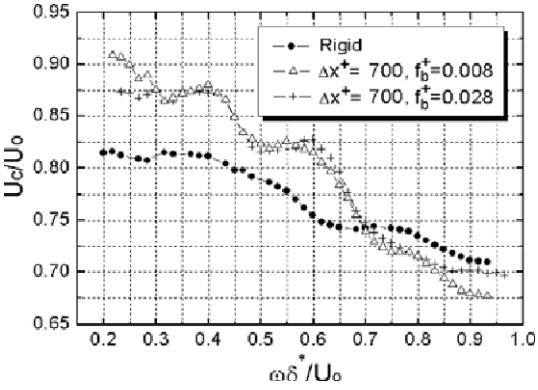

Fig. 14 Convection speed at each normalized frequency of wall-pressure spectrum by $700\nu/u_\tau$-long bimorph actuator

$\omega\delta^*/U_o \leq 0.35$ to move to the upper layer of higher speed than their normal convection speeds.

Figure 14 shows the significant increase of convection speed in the region of $\omega\delta^*/U_o \leq 0.7$ and the slight reduction of convection speed in the region of $\omega\delta^*/U_o > 0.7$ for the case of $700\nu/u_\tau$-long module. From this observation we may conclude that the large-scale structures satisfying $\omega\delta^*/U_o \leq 0.7$ is forced to move to the upper layer, accompanying a slight movement of the small-scale structures toward the wall due to the limitation of the sensor size. This movement of large-scale turbulent structures with possible deformation is considered to be the main mechanism of reduction in the wall-pressure energy spectrum by the local actuation of $700\nu/u_\tau$-long bimorph film.

3.3 Wall pressure characteristics in the latetransition boundary layer by active actuation

The wall pressure spectral level within the turbulent spot in the late-transitional boundary layer is known to be essentially same as that in fully turbulent boundary layer. The local forcing with considering the phase obtained by sensing the event was observed to be more effective for control than the simple actuation without consideration of the phase in the late-transitional boundary layer.

Table 3 shows the summary of boundary layer characteristics and control parameters. The bimorph actuator, which was located 700mm downstream from the leading edge, experienced late-transition there at an external speed of 9.27 m/s. The 1/8″ pressure-type microphone sensor is located 5mm upstream from the actuator, and its signal is conditioned to start the actuation. The time delay is computed from the convection speed of the temporal-spatial spectrum at the same time.

Table 3 Boundary layer characteristics and control parameters

U_o (m/s)	9.27
Re_θ	710
Shape factor	2.05
Delay time (sec)	0.001
Threshold voltage (volt)	0.1
Output voltage range (volt)	100

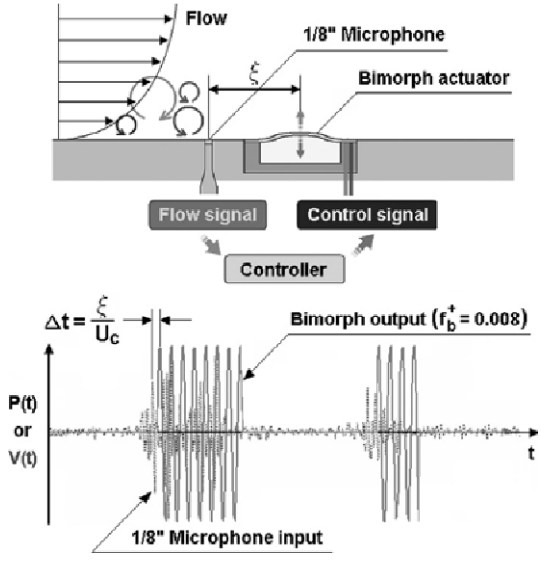

Fig. 15 Measured time signals by 1/8″ microphone and bimorph-actuator output signals

Figure 15 shows the instantaneous response of the bimorph film applied with about 100 V when the intermittent spots were sensed. The threshold for the input signal was set to 1.0V to clearly identify the intermittent spots rather than the mean fluctuating value. This setting is supported

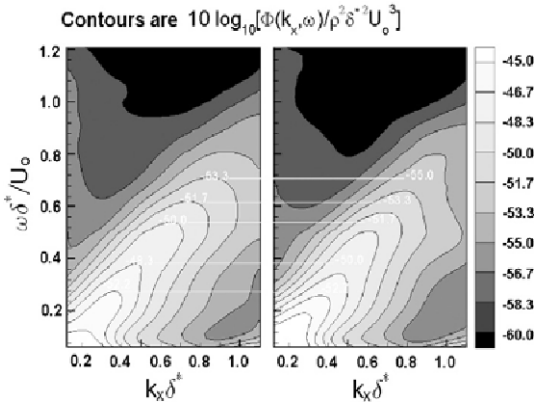

(a) w/o control (b) with control

Fig. 16 Temporal-spatial spectra of wall pressures in transitional boundary layer

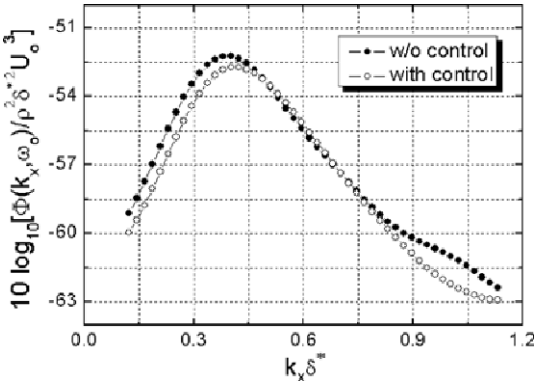

Fig. 17 Wall-pressure energies in terms of normalized wavenumber at $\omega\delta^*/U_o=0.3$ ($f=250$ Hz)

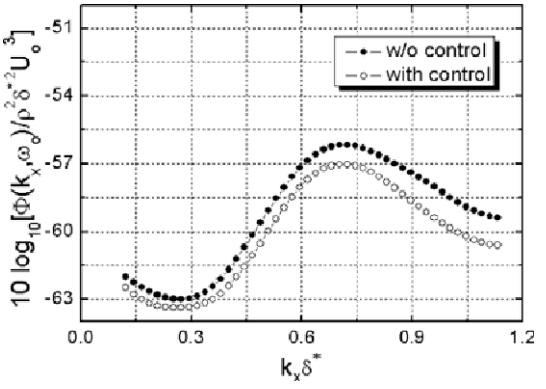

Fig. 18 Wall-pressure energies in terms of normalized wavenumber at $\omega\delta^*/U_o=0.6$ ($f=500$ Hz)

by the method of conditioning large-amplitude events in the fully turbulent flow, which are believed to contribute to the total energy of unsteady pressures dominantly.

Figure 16 shows the temporal-spatial spectra of wall pressures activated by the $700\nu/u_\tau$-long module at the frequency $f_b^+=0.008$ after sensing of the spots. They are also compared with that of solid surface without active forcing in the figure. The energy reduces in the convection ridge region of $k_x\delta^*>0.4$ for the case of actuation, as shown in the figure. The development toward turbulent boundary layer is temporarily delayed from the local reduction of the convecting energy by active forcing.

The wall pressure energies in the normalized wavenumber are compared at $\omega\delta^*/U_o=0.3$, 0.6 for the forcing and the non-forcing cases in Figs. 17 and 18, respectively. The forcing case of $f_b^+=0.008$ results in the maximum energy reduction of 0.87 dB near the convection wavenumber $k_x\delta^*=0.7$ for the case of $\omega\delta^*/U_o=0.6$, as shown in Fig. 18.

4. Conclusions

In this study, two actuators of piezoelectric bimorph films having the dimension of $1400\nu/u_\tau$ or $700\nu/u_\tau$ placed in the streamwise direction were designed and applied to the local wall in the boundary layer flow. The change of temporal-spatial spectra of wall pressures, activated by both modules at the frequency $f_b^+=0.008$ and 0.028, were compared with that of solid surface case without forcing. The reduction of wall-pressure spectral energy results from the fact that the large-scale structures satisfying $\omega\delta^*/U_o\leq0.7$ is forced to move to the upper layer by the local actuation of the $700\nu/u_\tau$-long bimorph film at the frequency $f_b^+=0.008$ and 0.028. The wall pressure characteristics by the local-displacement actuation were more dominantly influenced by the size of actuator module than the actuation frequency. The spanwise size of actuators, which is much wider than the average spacing of streaks near the wall, is considered to make the actuation frequency play an unimportant role for the re-

duction of wall-pressure spectral energy in this study.

The wavenumber-frequency spectra of wall pressure measured by the sensor array located downstream from the bimorph module of $\Delta x^+ = 700\nu/u_\tau$, the actuation of which is based on sensing of the event from the turbulent spot, showed the local reduction of convecting energy in the area of $k_x\delta^* > 0.4$.

The local forcing with considering the phase obtained by sensing the event was applied to the late-transitional boundary layer. The wall-pressure energy in the late-transitional boundary layer is partially reduced near the convection wavenumber by the open-loop control based on the recognition of the large-amplitude event by the turbulent spot.

Acknowledgements

This research was supported by the Grant No. R01-2004-000-10041-0 from the Basic Research Program of the Korea Science & Engineering Foundation.

References

Abraham, B. M. and Keith, W. L., 1998, "Direct Measurements of Turbulent Boundary Layer Wall Pressure Wavenumber-Frequency Spectra," *ASME J. Fluids Eng.*, Vol. 20, pp. 29～39.

Blackwelder, R. F. and Haritonidis, J. H., 1983, "Scaling of the Bursting Frequency in Turbulent Layers," *J. Fluid Mech.*, Vol. 132, pp. 87～103.

Choi, H. and Moin, P., 1990, "On the Space-Time Characteristics of Wall-Pressure Fluctuations," *physics of Fluids A*, Vol. 2, pp. 1450～1460.

Collis, S. S., Joslin, R. D., Seifert, A. and Theofilis, V., 2004, "Issues in Active Flow Control : theory, control, simulation and experiment," *Progress in Aerospace Sciences*, Vol. 40, pp. 237～289.

Farabee, T. M. and Casarella, M. J., 1991, "Spectral Features of Wall Pressure Fluctuations Beneath Turbulent Boundary Layers," *physics of Fluids A*, Vol. 3, pp. 2410～2420.

Gad-el-Hak, M., 2000, Flow Control, Cambridge University Press.

Jacobson, S. A. and Reynolds, W. C., 1998, "Active Control of Streamwise Vortices and Streaks in Boundary Layers," *J. Fluid Mech.*, Vol. 360, pp. 179～211.

Jeon, W.-P. and Blackwelder, R. F., 2000, "Perturbations in the Wall Region Using Flush Mounted Piezoceramic Actuators," *Exps. Fluids*, Vol. 28, No. 6, pp. 485～496.

Keith, W. L. and Bennett, J. C., 1991, "Low Frequency Measurements of the Wall Shear Stress and Wall Pressure in a Turbulent Boundary Layer," *AIAA*, Vol. 29, No. 4, pp. 526～530.

Landahl, M. T., 1975, "Wave Mechanics of Boundary Layer Turbulence Layer," *J.A.S.A.*, Vol. 57, pp. 824～831

Lee, S. and Kim, H.-J., 1999, "Experimental Study on Wall Pressure Fluctuations in the Turbulent Boundary Layer on a Flat-Plate," *J. KSME*, Part B, 23, No. 6, pp. 722～733.(in Korean)

Powell, A., 1960, "Aerodynamic Noise and the Plane Boundary," *J.A.S.A.*, Vol. 32, pp. 982～990

Smith, B. L. and Glezer, A., 1998, "The Formation and Evolution of Synthetic Jets," *physics of Fluids*, Vol. 10, pp. 2281～2297.

Wang, M., Lele, S. K., Moin, P., 1996, "Sound Radiation during Local Breakdown in a low Mach-number Boundary Layer," *J. Fluid Mech.*, Vol. 319, pp. 311～328

Wehrmann, O. H., 1965, "Reduction of Velocity Fluctuations in a Kármán Vortex Street by Vibrating Cylinder," *physics of Fluids*, Vol. 8, pp. 760～761.

Wehrmann, O. H., 1967, "Self-Adjusting Feedback Loop for Mechanical Systems to Influence Flow in Transition. Part I," Boeing Scientific Research Lab., Document D1-82-0632.

Wiltse, J. M. and Glezer, A., 1993, "Manipulation of Free Shear Flows Using Piezoelectric Actuators," *J. Fluid Mech.*, Vol. 249, pp. 261～285.